Modification of the Surface Properties of Polyimide Films using POSS Deposition and Oxygen Plasma Exposure

Christopher J. Wohl[1,*], *Marcus A. Belcher*[2], *Sayata Ghose*[2], *John W. Connell*[3]

[1]NASA Postdoctoral Fellow at NASA Langley Research Center, Hampton, VA 23681-2199

[2]National Institute of Aerospace, Hampton, VA 23666-6147

[3]NASA Langley Research Center, Hampton, VA 23681-2199

christopher.j.wohl@nasa.gov

RECEIVED DATE (to be automatically inserted after your manuscript is accepted if required according to the journal that you are submitting your paper to)

POSS-modified Polyimide Surfaces

Topographically rich surfaces were generated by spray-coating organic solutions of a polyhedral oligomeric silsesquioxane, octakis(dimethylsilyloxy)silsesquioxane (POSS), on Kapton® HN films and exposing them to radio frequency generated oxygen plasma. Changes in both surface chemistry and topography were observed. High-resolution scanning electron microscopy indicated substantial modification of the POSS-coated polyimide surface topographies as a result of oxygen plasma exposure. Water contact angles varied from 104° for unexposed POSS-coated surfaces to ~5° for samples exposed

for 5 h. Modulation of the dispersive and polar contributions to the surface energy was determined using van Oss Good Chaudhury theory.

Introduction

Materials with controllable surface properties show promise in a variety of applications. Anti-fouling and self-cleaning surfaces are often realized by low surface energy materials, while increases in surface energy can lead to adhesion promotion. Changes in either the surface chemistry or topography, or both, can have a dramatic impact on a given material's surface energy.

Nature has provided researchers with a self-cleaning system that is not only remarkably efficient, but also has a physical basis that can be emulated by man-made systems. This is perhaps best illustrated by leaves of the lotus plant, *Nelumbo nucifera.*[1] Studies of lotus leaves and similar botanical systems have established that the lotus plant's self-cleaning ability (e.g. the observed superhydrophobicity of the leaves) is dependent on both surface chemical composition and topography.[2] Hydrophobic waxy material and dual length-scale topographies (micrometer-sized protuberances and nano-scaled surface textures) enable these natural materials to exhibit self-cleaning properties.[3] Different methodologies have been developed to produce materials with high contact angles, including deposition of hydrophobic materials onto templated surfaces,[4-6] dual-length scale topographies generated by deposition from suspensions,[7, 8] and dissolution processes from complex mixtures.[9-11]

Conversely, adhesion promotion is achieved by generating an adherend with a surface energy that surpasses that of the adhesive.[12] Increased surface energy improves surface wettability, thereby promoting stronger adhesion between two surfaces. Surface modification procedures, such as grit-blasting, manual abrasion by sandpaper, chemical etching, flaming, electron beam irradiation, excimer laser irradiation, corona treatment, and plasma treatment, among other techniques, can improve wettability by raising a material's surface energy and improving the adhesive characteristics by creating bonding sites. However, reproducibility is often an issue with chemical etching and manual abrasion techniques as these can also be operator dependent processes. Even more rigorously controlled treatments, such as those by laser, corona, or plasma, can vary due to any of several factors. Exposure

of photochromic-containing materials to light has also been shown to reversibly change surface wettability.[13, 14]

The generation of self-cleaning surfaces would be beneficial for both manned and unmanned missions on the lunar surface.[15] While lunar soil (regolith) covers the entire surface of the Moon and is being pursued as a resource (i.e., *in-situ* resource utilization, ISRU), it is also hazardous to both astronauts and equipment.[16] Regolith consists of a broad array of different sized particles, with micrometer sized lunar dust comprising a significant fraction that is potentially the most problematic.[17] Lunar dust is produced from space weathering (meteorite impacts, radiation and thermal cycling) and, to a lesser degree, abrasion mechanisms due to the lunar surface dynamics of dust particles.[18-21] Astronauts from the Apollo missions observed the dynamic motions of dust particles as streaks in the sky near the terminator[22] and sub-micrometer sized lunar dust particles are thought to travel as high as 100 kilometers from the lunar surface.[19] Nano-scaled Fe^0 domains imparting magnetic properties to a substantial portion of the lunar dust have also been observed.[23] The lunar dust also presents health concerns.[24] Inhalation of lunar dust occurred during the Apollo 17 mission after astronauts removed their helmets and resulted in respiratory distress.[25]

Active mitigation strategies, techniques that involve the use of external stimulus, to address dust adhesion to lunar surface systems are currently being explored.[26, 27] However, passive lunar dust mitigation materials have not been developed. Therefore, one objective of this work is to generate a material with surface properties that could enable passive lunar dust mitigation (i.e. reduction in surface energy and available surface area).

In this work, the polyhedral oligomeric silsesquioxane, octakis(dimethylsilyloxy)-silsesquioxane (POSS, Scheme 1) is used to generate surface topography on polyimide films. POSS molecules were selected due to: 1) the presence of eight reactive silane bonds available to chemically bond to an activated Kapton® HN surface, 2) the stability of POSS-containing materials in highly oxidative environments,[28-30] and 3) the chemical composition of a POSS molecule which is intermediate (SiO_X) between that of silicone ($-R_2SiO-$) and silica (SiO_2) suggesting that POSS coatings may enhance

environmental stability and surface durability. The sample topography was modified by first activating the polyimide surface by exposure to oxygen plasma followed by spray-coating an organic solution of POSS and then additional oxygen plasma exposure. This methodology demonstrates a facile way to generate and alter surface features for use as potential lunar dust mitigating materials or adhesion promoters depending on the sample preparation protocol employed. Surface characterization was conducted using optical microscopy and high-resolution scanning electron microscopy (HRSEM). Variation of the material's surface chemistry was monitored using attenuated total reflection infrared (ATR-IR) spectroscopy, x-ray photoelectron spectroscopy (XPS), thermal gravimetric analysis (TGA), energy dispersive spectroscopy (EDS), and contact angle goniometry. Surface energy contributions from dispersive and polar interactions were identified using van Oss Good Chaudhury theory.

Scheme 1. Structure of octakis(dimethylsilyloxy)silsesquioxane, POSS (A), Kapton® HN (B) and suggested bonding interactions between POSS and activated Kapton® HN surface (C). Intermolecular bond formation (blue) and oxidative reactions (red) are both reasonable in an oxygen plasma environment. Additionally, oxidation reactions could result in opening of the POSS cages (not shown).

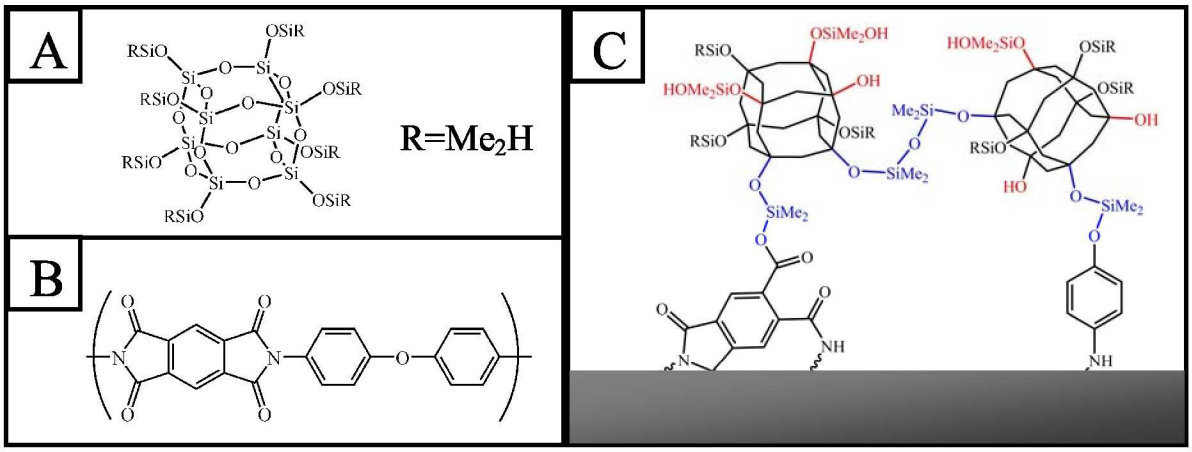

Materials and Methods

Materials. Kapton® HN (50.8 micrometers (2 mils), DuPont) was wiped with ethanol prior to surface treatments of any kind. Octakis(dimethylsilyloxy)silsesquioxane (POSS, Hybrid Plastics Inc.) was used

as received. Oxygen plasma was created using a Plasma Prep™ II Plasma Etcher (Structure Probes Inc.) at 100 W. Attenuated total reflection infrared (ATR-IR) spectra were recorded with a Thermo Nicolet IR300 spectrometer. X-ray photoelectron spectra (XPS) were recorded with a Kratos Axis 165 with an Al source. TGA were performed using a Netzsch TG 209 F1 under an air flow at 10 °C min^{-1} heating rate. Contact angle goniometry was performed using a FTA 1000B (First Ten Angstroms). Optical micrographs were collected using an Olympus BH-2 microscope equipped with a Hitachi KP-D50 digital color camera. HRSEM images were collected on a Hitachi S-5200 Field Emission High Resolution Scanning Electron Microscope equipped with a through the lens (TTL) detector and an EDS detector (EDAX, Mahwah, New Jersey). Due to poor conductivity and to enable EDS measurements (requiring > 10 kV), all SEM samples were sputter-coated with a ~10 nm thick gold/palladium film.

POSS-coated Kapton® HN Sample Preparation. Kapton® HN samples were exposed to oxygen plasma to "activate" the Kapton® HN surface prior to POSS deposition. Initial experiments conducted without this "activation step" resulted in highly heterogeneous POSS surface coverage (likely due to the low surface energy of pristine Kapton® HN). Exposure times were varied between 30 min and 2 h with 1 h providing the best results (i.e., leading to more uniform wetting). Subsequently, all samples were exposed to oxygen plasma for 1 h prior to POSS deposition. For clarity, "pristine Kapton® HN" will refer to samples that were not subjected to any oxygen plasma exposure for the purpose of surface activation, "activated Kapton® HN" will refer to samples that were exposed to 1 h of oxygen plasma prior to POSS deposition and "POSS-coated Kapton® HN" will refer to activated Kapton® HN spray-coated with POSS unless otherwise indicated. POSS was deposited on activated Kapton® HN surfaces from a 1 wt % THF solution using a Badger Model 250 mini spray gun in consecutive treatments, allowing the THF to evaporate between passes. The typical Kapton® HN sample size was a 5 cm x 5 cm square. For oxygen plasma exposure, specimens were placed in the middle of the plasma chamber to achieve a more uniform plasma density. Once "activated" samples were removed from the plasma chamber, POSS deposition was performed within 30 sec to prevent passivation of the activated Kapton® HN surface from ambient moisture. Samples were then exposed to oxygen plasma in 30 min increments

up to the specified cumulative time. Pristine Kapton® HN samples were exposed to oxygen plasma for the same duration as POSS-coated Kapton® HN samples to compare and characterize the exposure effects on the topography of the two surfaces.

Contact Angle Goniometry. Sessile drop contact angles were measured for each sample using a 3 μL drop of either water or ethylene glycol, or a 2 μL drop of diiodomethane. Interfacial tension measurements of a suspended drop of each liquid were made prior to experimentation to verify the purity of the liquid and precision of the focused image. The contact angles were determined by drop shape analysis and standard deviations were calculated by comparison of the contact angles observed for each frame of a 40 frame movie collected after drop deposition on the sample surface. Each sample was measured at least twice.

Results

Kapton® HN "Activation" and POSS Deposition. Pristine Kapton® HN surfaces were not well "wetted" by THF and this led to the formation of rounded clusters of POSS and heterogeneous surface distributions. To enhance the wettability of the pristine Kapton® HN surface, films were exposed to 1 h of oxygen plasma generating reactive surface groups (ketone, aldehyde, ester, and carboxylic acid functionalities can arise from bond scission and insertion processes),[31] enhancing surface wettability, and generating potential reaction sites for the silane bonds present on the POSS molecule. Even after surface activation, when relatively large amounts of solution were deposited in a single treatment, solvent droplets would coalesce resulting in large pools and yield less uniform POSS deposition. Therefore, several small volume deposition cycles were implemented enabling more homogeneous POSS deposition.

POSS-coated Kapton® HN Surface Topography. Optical microscopy and high resolution scanning electron microscopy (SEM) were used to observe variations in surface topography as a result of POSS

deposition, oxygen plasma exposure, or both. Changes to surface topography due to long-term oxygen plasma exposure on pristine Kapton® HN are well documented.[32-41] However, to delineate the effects of oxygen plasma exposure on pristine Kapton® HN and POSS architectures in this work, images were collected of pristine Kapton® HN exposed to oxygen plasma without POSS deposits. Oxygen plasma exposure increased the surface roughness of pristine Kapton® HN with increasing exposure time. Pristine Kapton® HN exposed to oxygen plasma for 60 min (Figure 1B) resulted in the formation of small rounded features (5 – 15 nm) and aggregate structures (35 – 60 nm). Extended exposure (90 min, Figure 1C) predominantly revealed single particulates on the surface with populations in two different size regimes, 15 – 30 nm and 50 – 70 nm.

At long exposure times (5 h), complete sample degradation was observed near the sample edges and small holes were observed throughout the sample. Similarly, residual organic debris resulting from reaction with the oxygen plasma covered large portions of the surface and formed closed roughly circular rings (Figure 1D). The presence of this organic residue provided some protection for the underlying material, while its surroundings continued to etch away due to differences in erosion rates. The diameter of these rings varied greatly (100 nm – 3 μm) with smaller rings more heavily populating the surface.

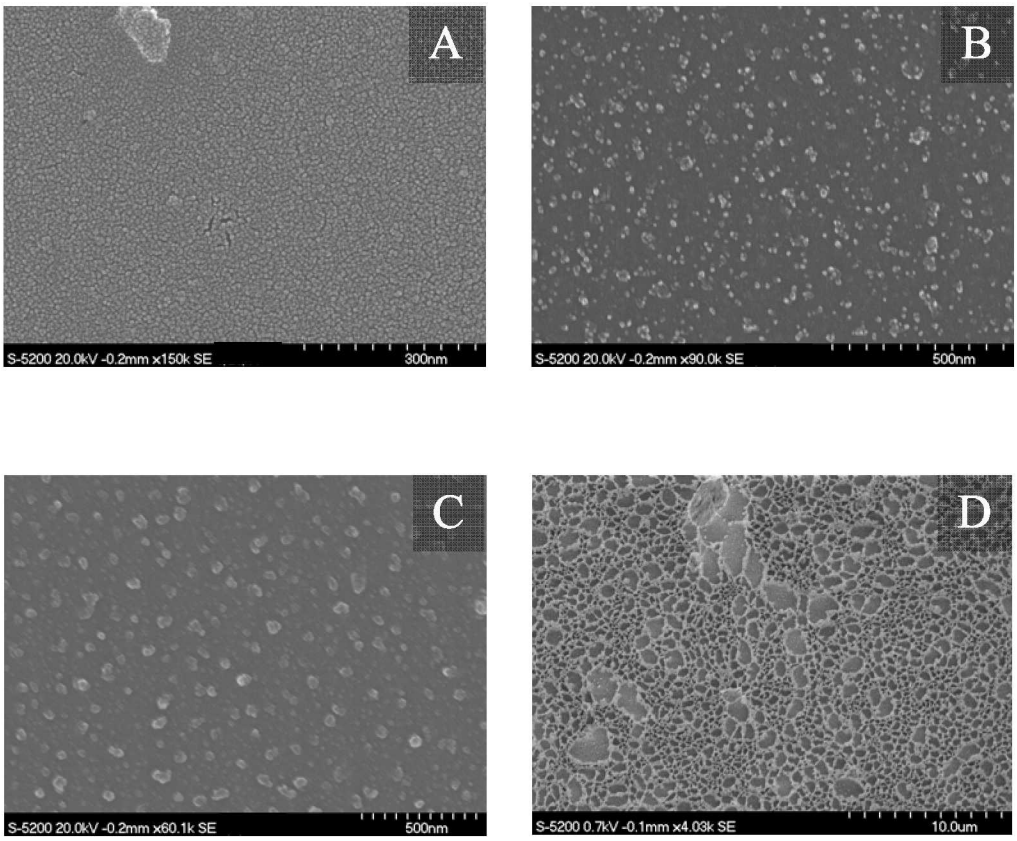

Figure 1. HRSEM images of pristine Kapton® HN with exposure to oxygen plasma for 0 min (A), 60 min (B), 90 min (C), and 5 h (D). The introduction of surface topography due to Au/Pd sputtering can be seen in (A). Exposure to oxygen plasma resulted in the appearance of surface features larger than the sputter material (B and C). The size of these features increased with exposure time. Continued exposure to oxygen plasma resulted in the formation of a network of organic debris that appeared to erode at a slower rate (D). Regions not covered by this organic layer continued to be etched and resembled the topography observed in (C).

POSS deposited on activated Kapton® HN generated "fern-like" structures (10 – 100 μm), which were observed to be the dominant surface feature with "fronds" extending from "fern" stems (Figures 2). Areas with high concentrations of POSS appear as stacked ferns. Large circular POSS deposits with typical diameters of 10 – 100 μm, both irregular and uniform in appearance, were also observed. EDS analysis confirmed the introduced topographical features to be POSS as indicated by enriched silicon

populations (Figure 2E). The oxygen map was similarly augmented while the carbon map was depleted in areas exhibiting POSS deposit features (data not shown).

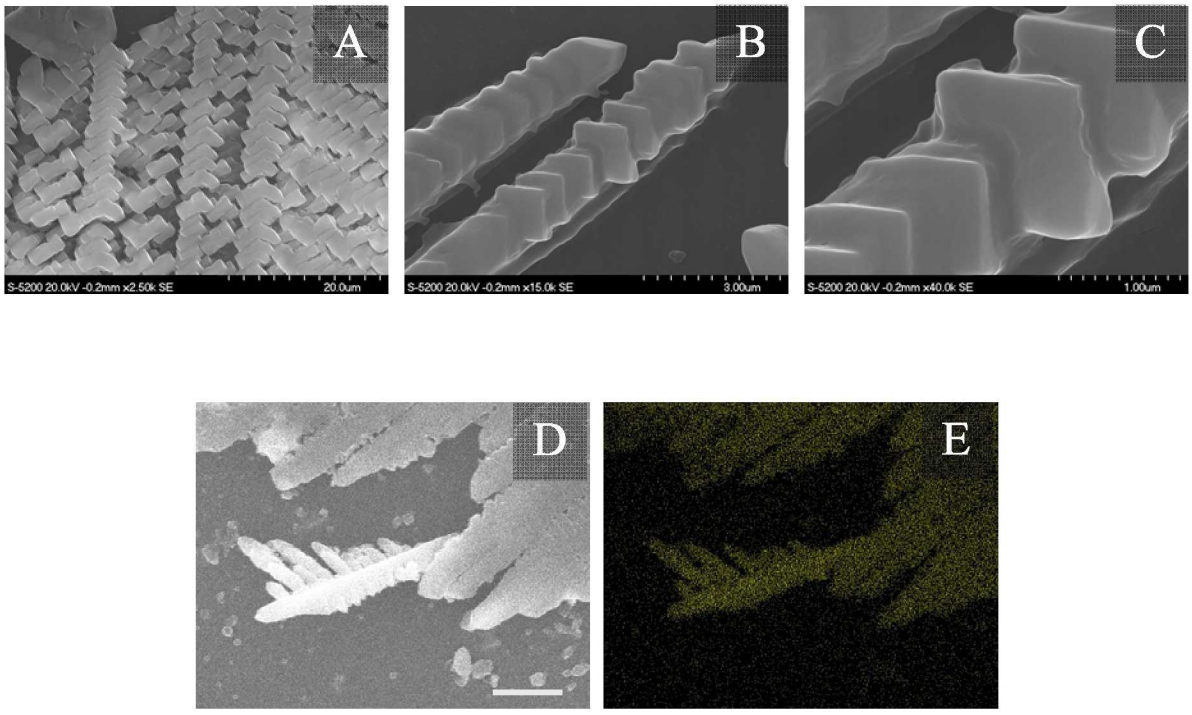

Figure 2. Fern-like structures were observed in areas of high POSS concentration on activated Kapton® HN and formed large POSS aggregates, which appeared to consist of a collection of "brick" and "boomerang" type structures (A). The discrete bricks were dimensionally consistent (4 μm by 2 μm). Bricks were frequently fused together forming the "blades" of the fern-like structures (B). The fused rectangular structures (C) are quite uniform, 1.0 – 1.5 μm long with approximately 750 nm of separation between rectangles. The thickness of the arms was typically 1.5 μm. The deposits observed in (D) are clearly traced out in the silicon EDS map (E). The small spherical particles in (D) did not appear on the Si map and could arise from the Kapton® HN itself as seen in Figure 1C. The scale bar in D is 5 μm. All images were taken of POSS-coated Kapton® HN.

Subsequent oxygen plasma exposure of POSS-coated Kapton® HN samples resulted in growth of tendril-like topographical features extending from the "fern" structures observed via optical microscopy

(Figure 3B). The length of these observed topographies appeared to increase with oxygen plasma exposure time and suggest that the silicate surface coverage was expanding due to oxygen plasma exposure. This may result in uniform surface coverage of activated Kapton® HN if the initial POSS deposition amount was sufficient. It is unclear what mechanism would cause POSS to migrate from regions of high POSS concentrations to regions of low POSS concentrations. POSS deposition/oxygen plasma exposure conditions for homogeneous POSS surface coverage are currently being evaluated.

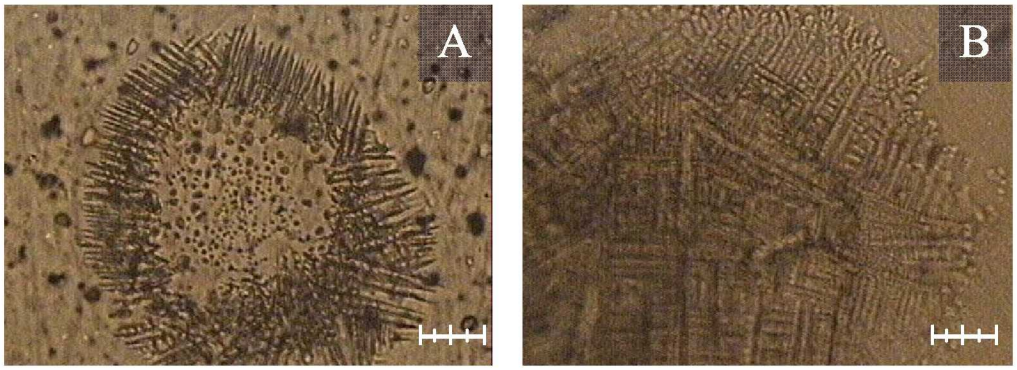

Figure 3. Optical photomicrographs of POSS-coated Kapton® HN. Sharp protrusions were observed to radiate from this spherical POSS deposit (A). Once exposed to oxygen plasma for 30 min, branched structures emanated from these protrusions (B). The scale bar in both images is 20 μm.

A broad expanse of fern-like POSS deposits with irregular growths similar to those depicted in Figure 3B is seen in the HRSEM image of POSS-coated Kapton® HN exposed for 30 min in Figure 4A. Expansion of this topography could be due to evaporation-condensation processes initiated by oxygen plasma exposure. Closer inspection reveals a surface with three distinct regions (Figure 4B). The brightest region corresponds to POSS deposits. These features are 200 – 400 nm thick and exhibit peak-like structures in the middle or at intersections possibly due to restructuring caused by oxygen plasma exposure. The space surrounding these POSS deposits appears to be polymeric material that has eroded due to oxygen plasma exposure. This region generally followed the contour of the POSS deposits and is similar in dimension (250 – 450 nm). Undercutting of the POSS deposits was also observed, similar to

that described previously.[42, 43] The polymer-POSS interface is likely an area with enhanced oxygen plasma erosion rates due to increased surface free energy. Finally, there is a region between the areas of enhanced polymeric erosion that appeared to be covered with a thin layer of silicate material. Tendril structures (Figure 4C, 8 ± 2 nm thick with intersection of features resulting in increased thickness) on POSS-coated Kapton® HN exposed to oxygen plasma appeared after much shorter exposure times compared to pristine Kapton® HN (see Figure 1D). Furthermore, apparent smoothing of the fern-like structures occurred after 1 h of oxygen plasma exposure (Figure 4D) and large circular deposits transformed to a more uniform coverage comprised of cracked platelets.

Long-term (≥ 2 h) oxygen plasma exposure of POSS-coated Kapton® HN surfaces resulted in additional topographical modifications. Holes developed in POSS deposits (< 400 nm) and large sections of the deposits (up to 1 μm) appeared to be removed as oxygen plasma exposure times increased (Figures 4E and 4F). It is plausible that holes in the POSS deposits allowed degradation of the underlying polymeric material. Fern "fronds" and "blades" were reduced in size (800 ± 50 nm and 500 ± 100 nm, respectively) compared to deposits without oxygen plasma exposure (1500 ± 150 nm and 1000 ± 250 nm, respectively).

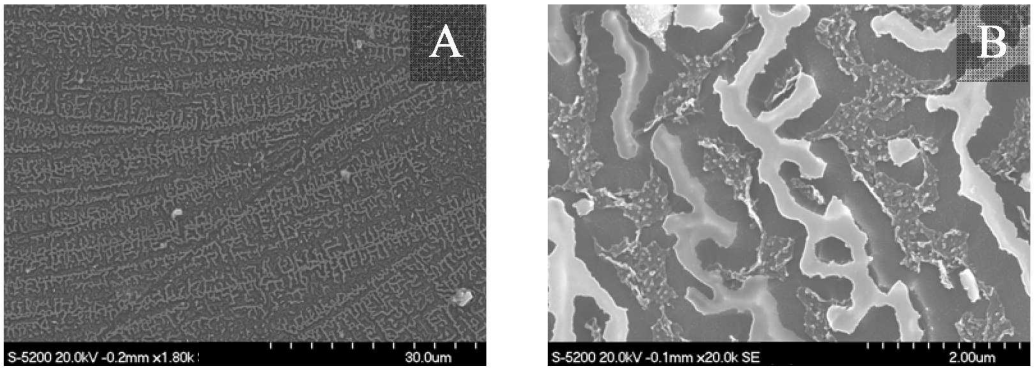

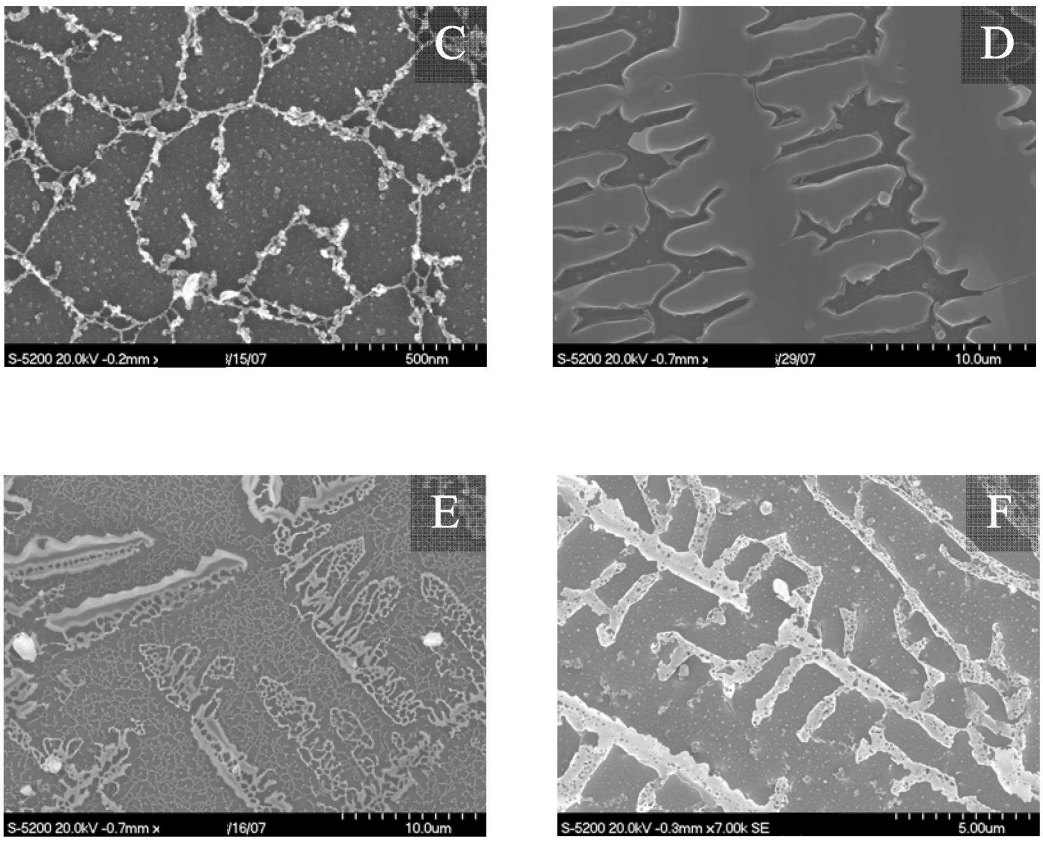

Figure 4. HRSEM images of POSS-coated Kapton® HN exposed to oxygen plasma for 30 min (A and B, where B is a magnified view of the structures seen in A). Initial stages of tendril growth could be seen after only 30 min of oxygen plasma exposure. Exposure for 1 h resulted in dramatic surface coverage and introduction of new topographical features (C) with the tendril network appearing to cover a majority of the surface after only 2 h of oxygen plasma exposure. 1 h of exposure also resulted in surface feature smoothing of the POSS deposits (D). After 4 h, the fern-like POSS structures displayed holes (E) and structural degradation (F).

Collectively, all of the discussed topographical features suggest that, at appropriate surface concentrations, POSS deposition can effectively produce a tailorable, topographically rich surface. As an example of the efficacy of this procedure, THF solutions of POSS were deposited drop-wise onto tunneling electron microscopy (TEM) grids placed on top of activated Kapton® HN samples. Optical and SEM images were collected before and after exposure to oxygen plasma for 1 h (Figure 5). Prior to

oxygen plasma exposure, the POSS deposits were well segregated according to the TEM template (Figure 5A and C); however, after exposure to oxygen plasma, branching between POSS deposits was observed (Figure 5B) and the smooth appearance of the activated Kapton® HN surface between POSS deposits was replaced with topographical features (Figure 5D).

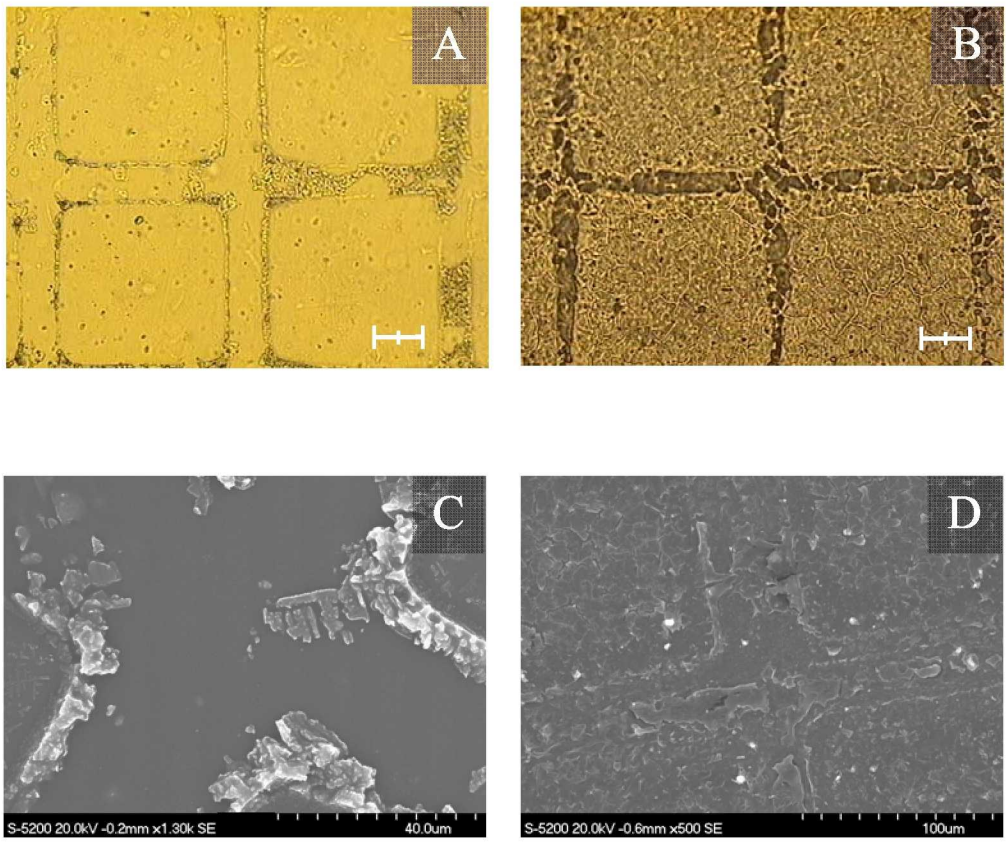

Figure 5. Optical Microscope (A and B) and SEM (C and D) images of POSS deposited on activated Kapton® HN using a TEM grid template. The ordered POSS deposit structures prior to additional oxygen plasma exposure (A and C) were replaced with branching (B) and topographical features (D) after 1 h of oxygen plasma exposure. Scale bars in A and B are 40 μm.

Oxygen Plasma Exposure Effects on Surface Chemistry. Exposure of POSS-coated Kapton® HN to oxygen plasma can initiate two different chemical reaction pathways. First, the polymer surface could undergo further oxidation and react with the eight reactive silane (Si-H) bonds of each POSS molecule.

Secondly, exposure to oxygen plasma could result in direct oxidation of either the Si-H bonds or POSS cages themselves resulting in surface materials with a chemical composition approaching that of silica (SiO_2).

The disappearance of Si-H stretching vibrations observed for POSS molecules was monitored as a function of oxygen plasma exposure via ATR-IR. The absorbance ratio of two characteristic POSS vibrations, the Si-H stretch ($\nu = 2140\ cm^{-1}$) and the Si-O-Si stretch ($\nu = 1068\ cm^{-1}$), was calculated as a function of oxygen plasma exposure time to assess the degree of Si-H bond reaction. These IR-active modes were chosen because they involve the functional group of interest, the Si-H bond, and are resolved from the spectral features of pristine Kapton® HN. There is a dramatic reduction in the Si-H stretch intensity upon extended oxygen plasma exposure of POSS-coated Kapton® HN samples (Figure 6). After 1 h, the absorbance ratio reached a minimum. If we assume the degree of Si-O-Si bonding to be relatively constant, this could indicate a maximal time of non-destructive topographical modification arising from reaction of Si-H bonds with the activated Kapton® HN surface, other POSS molecules, or reactive species in the oxygen plasma itself. However, Si-O-Si bonding could increase as a result of oxygen plasma exposure and resultant POSS decomposition. While it is not possible to accurately differentiate between the disappearance of Si-H bonds and generation of Si-O-Si bonds in these spectra, it is likely that the formation of any additional Si-O-Si features arose, at least partly, from the reaction of Si-H functionalities.

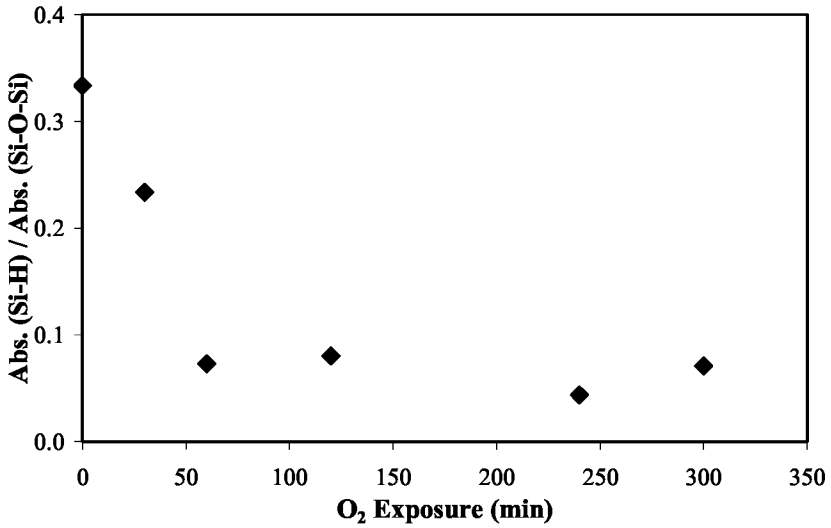

Figure 6. The ratio of Si-H and Si-O-Si vibrational bands using ATR-IR spectroscopy indicated a rapid disappearance of Si-H functionalities due to oxygen plasma exposure. Exposures longer than 1 h did not reduce this ratio, within experimental uncertainty, suggesting that a majority of the Si-H bonds present on the POSS molecules had reacted in the oxygen plasma.

Further information regarding changes in surface chemistry was obtained by XPS analysis. The XPS spectrum for a POSS-coated Kapton® HN sample indicated that the major contributors for the Si_{2p} signal corresponded to two different binding energies, 101.3 and 102.7 eV (Table 1). These peaks correlate to the two different Si bonding configurations present in POSS: that is, a silicon atom bound to two carbons, one oxygen and one hydrogen atom, and a silicon atom bound to four oxygen atoms, respectively. The XPS spectrum for POSS-coated Kapton® HN samples exposed to 1 h of oxygen plasma displayed similar binding energies for the Si_{2p} signal. Surprisingly, the magnitude of the lower energy peak increased with additional oxygen plasma exposure. This was unexpected as the oxidative environment present in oxygen plasma would be expected to increase the population of higher binding energy Si atoms. One explanation is that reactive groups on the polymer surface chemically bonded with the POSS molecules generating a greater population of lower binding energy materials. This is supported by reduction in Si_{2p} binding energies due to reduction in the Si oxidation state.[44, 45]

Combined with the IR data, these results suggest that POSS molecules are binding to the Kapton® HN surface through reaction between Si-H bonds and Kapton® HN surface functionalities.

Table 1. XPS Si_{2p} binding energies for POSS-coated Kapton® HN samples.

	Si_{2p} binding energy			
	101.3 eV		102.7 eV	
Oxygen plasma exposure (h)	FWHM	Relative % area	FWHM	Relative % area
0	1.45	17.9	1.61	82.1
1	1.57	58.7	1.40	41.3

TGA also indicated changes in the Kapton® HN and POSS interactions as a result of oxygen plasma exposure. The thermogram for POSS collected in air at 10 °C/min (Figure 7) exhibited a mass loss process initiated at approximately 200 °C, potentially corresponding to loss of the POSS molecule's organic functionalities,[46] while pristine Kapton® HN displayed mass loss beginning at 550 °C. For POSS-coated Kapton® HN samples, a small but significant mass loss event occurs at temperatures corresponding to the mass loss process observed for "neat" POSS (Figure 7, see inset). Once the POSS-coated Kapton® HN surface was exposed to oxygen plasma for 1 h this mass loss event disappeared. Stronger polymer-POSS interactions, possibly chemical bonding, could explain this observation in agreement with both XPS and ATR-IR data. The steady mass loss observed in the thermogram of POSS-coated Kapton® HN with 1 h of oxygen plasma exposure could result from the loss of polyimide residues formed during oxygen plasma exposure.

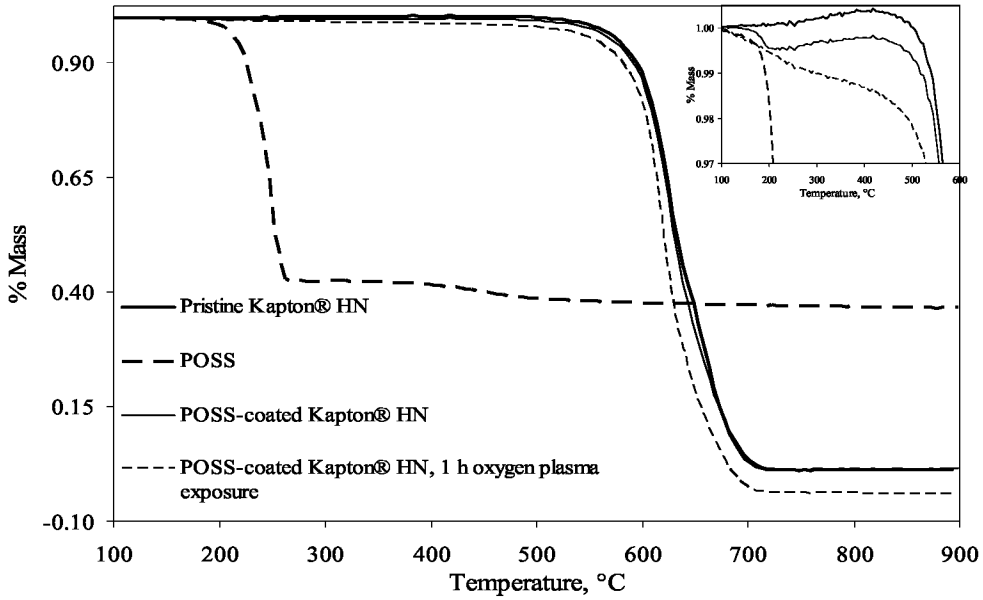

Figure 7. TGA thermograms illustrate the change in behavior of POSS deposits as a result of oxygen plasma exposure.

Contact Angle Analysis. Contact angle information was collected using three different liquids to delineate contributions to surface energy from specific intermolecular interactions. The Young-Dupree equation relates the observed contact angle of a liquid on a surface to the material's surface energy, γ_i^{tot}. van Oss Good and Chaudhury described the surface energy of a material as being the sum of dispersive, γ_i^D, and Lewis acid-base components, γ_i^{AB}:[47]

$$\gamma_i^{tot} = \gamma_i^D + \gamma_i^{AB} \tag{1}$$

where the Lewis acid-base component is defined as:

$$\gamma_i^{AB} = 2\left(\gamma_i^+ \gamma_i^-\right)^{1/2} \tag{2}$$

with γ_i^+ and γ_i^- being the acidic and basic contributions to the surface energy respectively. Thus, the Young-Dupree equation becomes:

$$\gamma_L^{tot}\left(1+\cos(\vartheta)\right) = 2\left(\gamma_L^D \gamma_S^D\right)^{1/2} + 2\left(\gamma_L^+ \gamma_S^-\right)^{1/2} + 2\left(\gamma_L^- \gamma_S^+\right)^{1/2} \tag{3}$$

Using Eq. 3, contact angle measurements must be made using three liquids, L, with known surface tension values to determine the individual surface energy contributions for a surface, S. Using water,

ethylene glycol, and diiodomethane, the surface energy contributions for the POSS-coated Kapton® HN samples were determined. The total surface energy decreased as a result of POSS deposition and increased dramatically upon exposure to oxygen plasma for Kapton® HN with and without POSS (Figure 8, top). The acid-base contributions to surface energy increased after oxygen plasma exposure for both surfaces (Figure 8, middle); however, the dispersive component decreased for pristine Kapton® HN. The oxygen plasma environment is oxidative and, therefore, increases in the basic component to the surface energy are not unexpected. Surprisingly, pristine Kapton® HN surfaces exhibited an increase in both the acidic and basic component due to oxygen plasma exposure (Figure 8C, bottom), while the basic component of POSS-coated Kapton® HN samples increased substantially with a concomitant decrease in the acidic component.

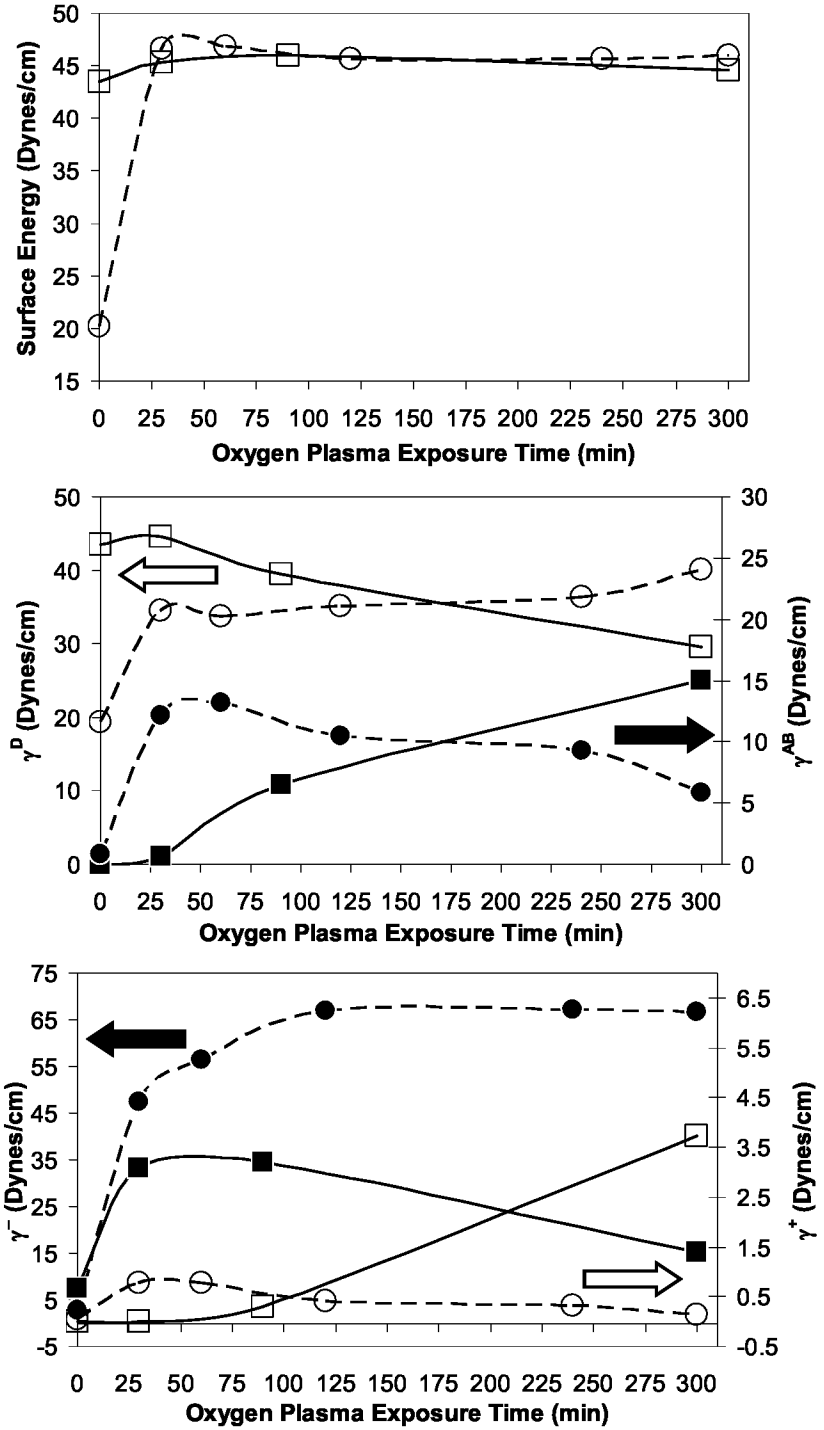

Figure 8. Oxygen plasma exposure effects on the total surface energy (top), dispersive and polar contributions (middle), and the acidic and basic contributions (bottom) of pristine Kapton® HN and POSS-coated Kapton® HN surface. Pristine Kapton® HN values and POSS-coated Kapton® HN values are represented by (□) and (○) respectively. Lines are drawn simply to aid in visualization and the arrows relate the appropriate data set to its axis.

Discussion

Exposure of Kapton® HN to oxygen plasma is known to result in material degradation processes. However, shorter oxygen plasma exposures can also enhance the surface properties of materials. Oxygen plasma exposure of pristine Kapton® HN used as an "activation" step prior to POSS deposition increased the surface energy as indicated by contact angle analysis and resulted in enhanced wettability of the POSS organic solution. This resulted in more uniform POSS deposition and greater surface coverage.

SEM images indicated that both POSS deposition and exposure to oxygen plasma resulted in modification of the surface topography of pristine Kapton® HN. The plausible impact of this on adhesion behavior can be determined using surface energy analysis. The dispersive component, which relies on available contact area, was observed to decrease after exposure to oxygen plasma or POSS deposition. In both scenarios, a reduction in the available surface area resulted in diminished dispersive intermolecular interactions suggesting that, at least for POSS-coated Kapton® HN, the surface may be described by a Cassie state. A droplet on a surface in a Cassie state experiences disruptions in the three-phase contact line due to air pockets trapped between the surface and the liquid. Exposure to oxygen plasma resulted in the spreading of surface features for POSS-coated Kapton® HN samples. This expansion of topography, along with changes in surface chemistry, increased the surface energy contributions from dispersive forces as indicated by contact angle measurements. This behavior implies that the surface transitioned from a Cassie state to a Wenzel state where the three-phase contact line is continuous.

Once POSS-coated Kapton® HN samples are exposed to oxygen plasma, chemical reactions could occur in addition to polyimide degradation processes. The silane functional groups can react with surrounding functionalities or the oxygen plasma (Scheme 1), as indicated by reduction in the Si-H vibrational band intensity, changes in the binding energy profile of the XPS Si_{2p} signal, and different responses to changes in thermal environment as indicated by TGA. A dramatic increase in the surface

energy occurred after only 30 min of oxygen plasma exposure. The acid-base contribution to surface energy increased significantly with the greatest change occurring for the basic component, an expected result due to the highly oxidative nature of oxygen plasma. The basic contribution of POSS-coated Kapton® HN samples exceeded that of pristine Kapton® HN after exposure to oxygen plasma. This behavior suggests that introduction of POSS deposits to the activated Kapton® HN surface may enhance adhesive interactions compared to pristine Kapton® HN.

Conclusions

Kapton® HN substrates were topographically modified by both oxygen plasma exposure and deposition of polyhedral oligomeric silsesquioxane molecules. Analytical techniques enabled the determination of not only the behavior of POSS molecules diffusing from THF solution to the polymer surface, but also changes in topography and chemistry as a result of oxygen plasma exposure. Deposition of POSS molecules introduced topography and resulted in surface energy reduction which could prove useful for lunar dust mitigation applications. Changes in the dispersive energy component indicated a transition from a Cassie to a Wenzel state for POSS-coated Kapton® HN surfaces due to oxygen plasma exposure. Furthermore, the basic contributions to surface energy were enhanced after POSS deposition and subsequent oxygen plasma exposure, indicating a possible increase in adhesive interactions as a result of these surface treatments. This approach is applicable to a variety of polymeric materials and testing is planned to assess both the lunar dust adhesion mitigation properties of the POSS-coated Kapton® HN surfaces and the enhanced adhesion properties of these surfaces once exposed to oxygen plasma.

Acknowledgement.

The authors would like to acknowledge Joan Hudson at the Clemson University Advanced Materials Research Labs EM Lab for performing the XPS measurements and Drs. Peter Lillehei at NASA Langley Research Center and Kent Watson at The National Institute of Aerospace for scientific and technical support. The authors also acknowledge funding from the Oak Ridge Associated Universities NASA Post-doctoral program and the Dust Project under the Exploration Science Mission Directorate (ESMD).

1. Barthlott, W.; Neinhuis, C., *Planta* **1997,** 202, (1), 1.
2. Neinhuis, C.; Barthlott, W., *Ann. Botany* **1997,** 79, 667.
3. Patankar, N. A., *Langmuir* **2004,** 20, (19), 8209.
4. Hassel, A. W.; Milenkovic, S.; Schurmann, U.; Greve, H.; Zaporojtchenko, V.; Adelung, R.; Faupel, F., *Langmuir* **2007,** 23, 2091.
5. Lee, J. A.; McCarthy, T. J., *Macromolecules* **2007,** 40, 3965.
6. Zhang, L.; Zhou, Z.; Cheng, B.; DeSimone, J.; Samulski, E., *Langmuir* **2006,** 22, 8576.
7. Li, Y.; Huang, X. J.; Heo, S. H.; Li, C. C.; Choi, Y. K.; Cai, W. P.; Cho, S. O., *Langmuir* **2007,** 23, 2169.
8. Wang, C. F.; Wang, Y. T.; Tung, P. H.; Kuo, S. W.; Lin, C. H.; Sheen, Y. C.; Chang, F. C., *Langmuir* **2006,** 22, 8289.
9. Chen, S.; Hu, C.; Chen, L.; Xu, N., *Chem. Commun.* **2007,** 19, 1919.
10. Ma, Y.; Cao, X.; Feng, X.; Ma, Y.; Zou, H., *Polymer* **2007,** 2007, (48), 7455.
11. Rioboo, R.; Voue, M.; Vaillant, A.; Seveno, D.; Conti, J.; Bondar, A.; Ivanov, D.; Coninck, J., *Langmuir* **2008,** 24, 9508.
12. Ebnesajjad, S.; Ebnesajjad, C., *Surface treatment of materials for adhesion bonding*. William Andrew Publishing: Norwich, NY, USA, 2006.
13. Rosario, R.; Gust, D.; Garcia, A.; Hayes, M.; Taraci, J.; Clement, T.; Dailey, J.; Picraux, S., *J. Phys. Chem. B* **2004,** 108, 12640.
14. Wang, S.; Song, Y.; Jiang, L., *J. Photochem. Photobiol., C* **2007,** 8, 18.
15. *NASA's exploration systems architecture study*. NASA/TM--214062; National Aeronautics and Space Administration: 2005.
16. Gaier, J., *The effects of lunar dust on EVA systems during the Apollo missions*. NASA/TM-213610; National Aeronautics and Space Administration: 2005.
17. Lee, L.-H., *J. Adhes. Sci. Technol.* **1995,** 9, (8), 1103.
18. Carrier, W. D.; Olhoeft, G. R.; Mendell, W., *Lunar sourcebook: A users guide to the moon*. Cambridge University Press: 1991.
19. Stubbs, T.; Vondrak, R.; Farrell, W., *Adv. Space Res.* **2006,** 37, 59.
20. Borisov, N.; Mall, U., *Planetary Space Sci.* **2006,** 54, 572.
21. Kolesnikov, E.; Yakovlev, A., *Planetary Space Sci.* **2003,** 51, 879.
22. Rennilson, J.; Criswell, D., *The Moon* **1974,** 10, 121.
23. Taylor, L.; Meek, T., *J. Aerospace Eng.* **2005,** 18, (3), 188.
24. Khan-Mayberry, N., *Acta Astronautica* **2008,** 63, 1006.
25. Goodwin, R., *Apollo 17: The NASA mission reports*. Apogee Books: Ontario, Canada, 2002; Vol. 1.
26. Immer, C.; Starnes, J.; Michalenko, M.; Calle, C.; Mazumder, M. Electrostatic screen for transport of Martian and Lunar regolith, In *Lunar and Planetary Science XXXVII Conference*, Lunar Planetary Institute: Houston, 2006; abstract # 2265.

27. Taylor, L.; Schmitt, H.; Carrier, W. D.; Nakagawa, M., The lunar dust problem: from liability to asset. In *1st Space exploration conference: continuing the voyage of discovery*, American Institute of Aeronautics and Astronautics: Orlando, Florida, 2005.
28. Augustine, B.; Hughes, W. C.; Zimmermann, K.; Figueiredo, A.; Guo, X.; Chusuei, C.; Maidment, J., *Langmuir* **2007,** 23, 4346.
29. Brunsvold, A. L.; Minton, T.; Gouzman, I.; Grossman, E.; Gonzalez, R. I., *High Perform. Polym.* **2004,** 16, 303.
30. Phillips, S.; Haddad, T.; Tomczak, S., *Curr. Opin. Solid State Mater. Sci.* **2004,** 8, 21.
31. Chan, C. M., *Polymer surface modification and characterization.* Carl Hanser Verlag: Munich, 1994.
32. Levine, A. LDEF-69 months in space: first post retrieval symposium, Part 1, National Aeronautics and Space Administration: Kissimmee, Florida, 1992; NASA -CP, 3134 (2).
33. Levine, A. LDEF-69 months in space: second post retrieval symposium, Part 1, National Aeronautics and Space Administration: San Diego, CA 1992; NASA-CP 10097.
34. Gerlach, L., *Ecol. Soc. Amer.* **1990,** 14, 149.
35. Hansen, R.; Pascale, J.; Benedictis, T.; Rentzepis, P., *J. Polym. Sci., Part A: Polym. Chem.* **1965,** 3, 2205.
36. Leger, J., *Oxygen atom reaction with shuttle materials at orbital altitudes.* NASA/TM--58246; National Aeronautics and Space Administration: 1982.
37. Leger, L.; Visentine, J.; Santos-Mason, B., *SAMPE Quarterly* **1987,** 18, (2), 48.
38. Stein, B. LDEF materials workshop-91, National Aeronautics and Space Administration: Hampton, VA, 1991; NASA-CP 3162.
39. Visentine, J. *STS-8 atomic oxygen effects experiments*, Atomic oxygen effects measurements for shuttle missions STS-8 and 41-G, Visentine, J., Ed. 1988; NASA/TM-100459 pp 2-1.
40. Zimcik, D.; Maag, C., *J. Spacecraft* **1988,** 25, (2), 162.
41. Snyder, A., *Investigation of atomic oxygen erosion of polyimide Kapton H exposed to a plasma asher environment.* NASA/TM-209178; National Aeronautics and Space Administration: 1999.
42. de Groh, K.; Banks, B., *J. Spacecraft Rockets* **1994,** 31, (4), 656.
43. Rutledge, S.; Mihelcic, J., *Surf. Coat. Technol.* **1989,** 39/40, 607.
44. Okada, K.; Kameshima, Y.; Yasumori, A., *J. Am. Ceram. Soc.* **1998,** 81, (7), 1970.
45. Rochet, F.; Dufour, G.; Roulet, H.; Pelloie, B.; Perriere, J.; Fogarassy, G.; Slaoui, A.; Froment, M., *Phys. Rev. B: Condens. Matter Mater. Phys.* **1988,** 37, (11), 6468.
46. Markovic, E.; Clarke, S.; Matisons, J.; Simon, G., *Macromolecules* **2008,** 41, 1685.
47. van Oss, C.; Giese, R.; Good, R., *Langmuir* **1990,** 6, 1711.